Developmental Cell

Supplemental Information for

Measuring pushing and braking forces generated by kinesin-5 crosslinking two microtubules

Yuta Shimamoto, Scott Forth, and Tarun M. Kapoor

Inventory of Supplementary Materials

Figure S1, related to Figure 1. Additional data for our in vitro force assay

Figure S2, related to Figure 2. Additional data for force generation of antiparallel microtubule pairs crosslinked by kinesin-5

Figure S3, related to Figure 4. Additional analyses of force development within antiparallel microtubule pairs that are slid apart at constant velocity

Figure S4, related to Figure 5. Additional analyses of parallel microtubule pairs crosslinked by kinesin-5

Figure S5, related to Figure 6. Model simulation results

Supplementary Experimental Procedures

Supplementary References

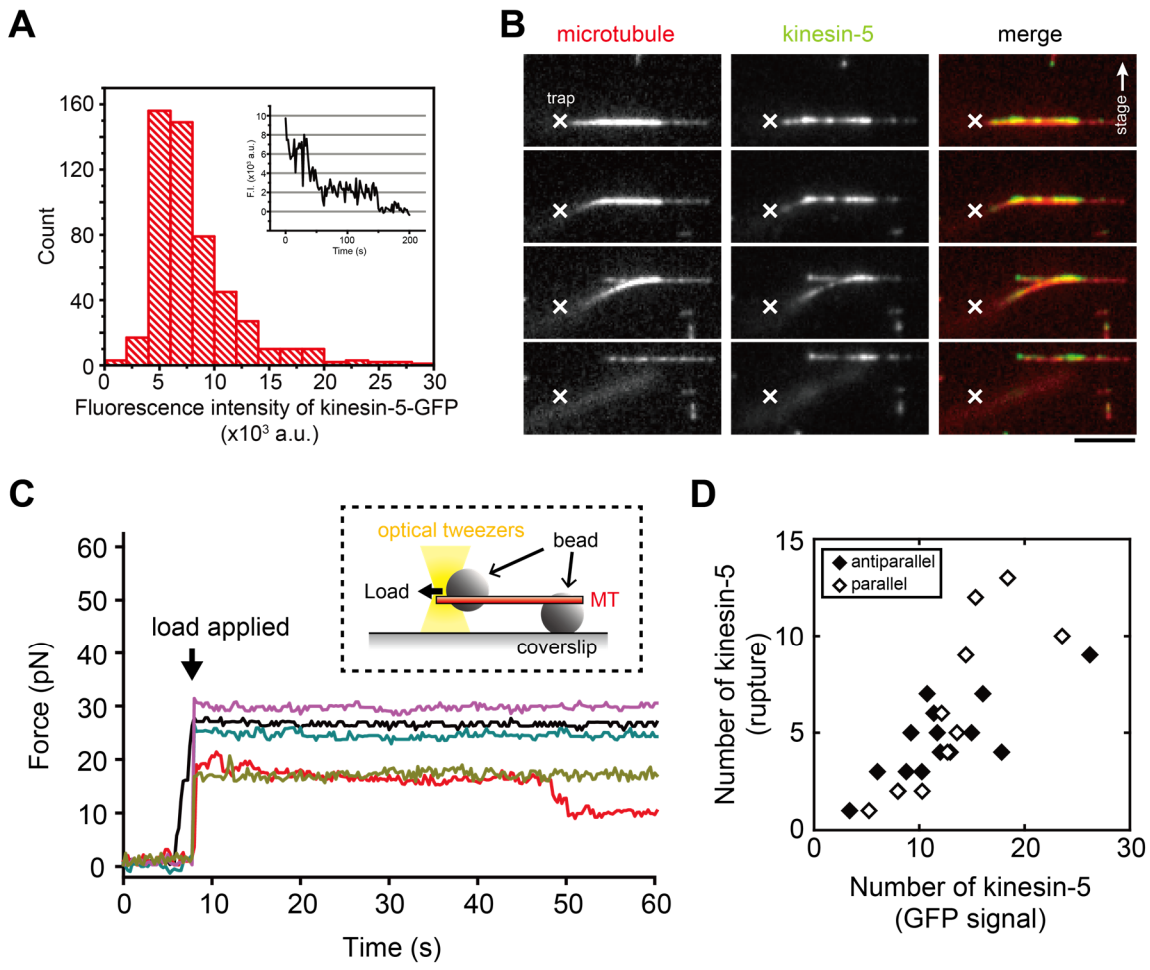

Figure S1. Additional data for our in vitro force assay, Related to Figure 1

(**A**) Analysis of the average fluorescence intensity of kinesin-5-GFP. Histogram showing the distribution of GFP signal intensity measured for n = 410 of the homotetrameric motor molecule. The motor protein construct was spread onto coverslip surface at a low density and the signal intensity of individual GFP fluorescence spots were measured. Inset shows a time-record of GFP signal from a single fluorescent spot, revealing stepwise photobleaching.

(**B**) Rupture-based analysis to estimate the number of kinesin-5 molecules crosslinking two microtubules. Time-lapse images show motions of microtubules and the localization of kinesin-5-GFP. In typical rupture analysis, the surface microtubule is moved orthogonal to the bead-attached microtubule, but slightly towards the trap position center. As a result, the trapped bead is further pushed away from trap center and the force increases accordingly. Once a crosslinking molecule ruptures, the strain relaxes and the bead is pulled back towards the trap center. The bead comes back to the trap center when the filaments are fully dissociated with each other. The rupture peaks are clearly observed parallel to the filament axis whereas the peaks perpendicular to the filament axis are typically very small. This is likely because the microtubule bends more easily in this direction. Scale bar, 5 μm.

(**C**) Strength of the bead-microtubule linkage. The stability of the bead-microtubule linkage was examined using an assay as shown in inset. One bead was fixed onto a coverslip surface while the other bead was captured by optical tweezers. Load was applied by moving the sample stage

in a step-wise manner (vertical arrow) and the subsequent response was measured. A sustained level of each force trace indicates that the bead-microtubule attachment can withstand tens of pN load (typically >30 s lifetime) without dissociation. The end compliance is also negligible (<1 pN change in 30 s). Note that the trap stiffness of 0.16 pN/nm was used in this assay to apply relatively large load.
(**D**) Comparison of kinesin-5 molecule counting using fluorescence and rupture-based analysis. Plots are of antiparallel (filled diamonds, n = 15) and parallel (open diamonds, n = 10) microtubule pairs, analyzed in Figure 2 and Figure 5, respectively.

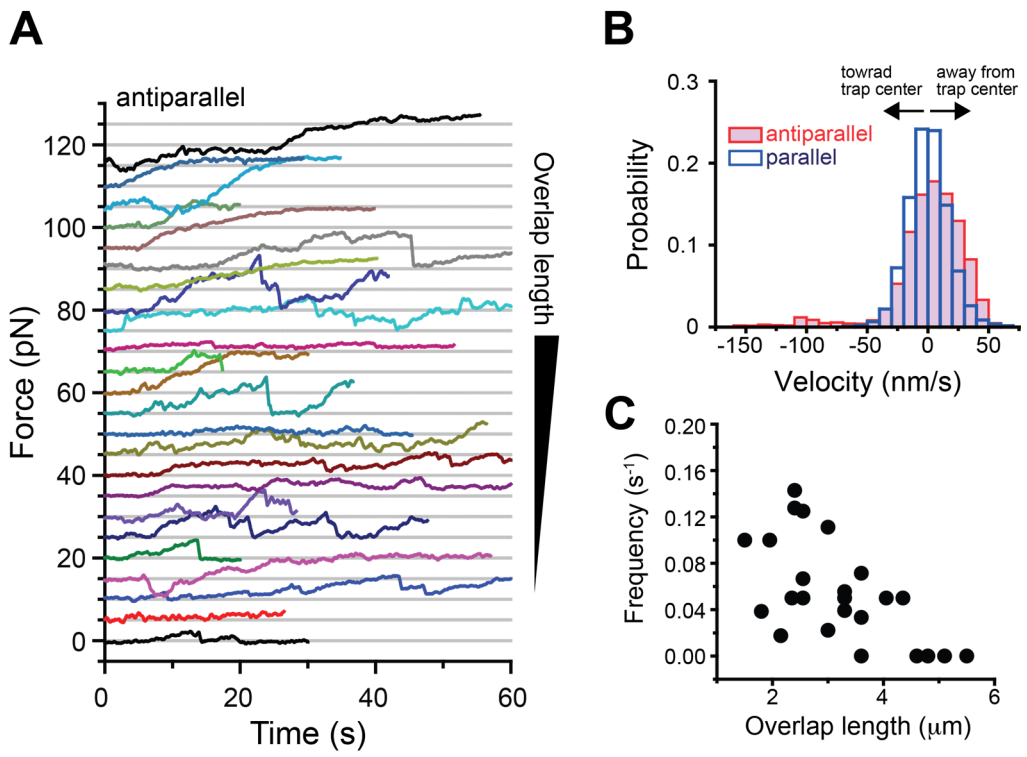

Figure S2. Additional data for force generation of antiparallel microtubule pairs crosslinked by kinesin-5, Related to Figure 2

(**A**) Records of force versus time obtained from antiparallel microtubule pairs of various overlap lengths. A trapped bead was attached at ~5 s and the subsequent force development was measured. For clarity, individual data plots are smoothened by a 200-ms moving average filter and displayed by 5 pN offset.

(**B**) Microtubule sliding velocity during the force development. Histogram shows a typical distribution of the relative filament sliding velocity, analyzed for an antiparallel microtubule pair generating force (red columns). The velocity was analyzed from the motion of the microtubule-attached optically-trapped bead. The right-side peak of the histogram (at 20-30 nm/s) corresponds to the microtubule motion pushing the bead away from trap center while the left-side peak (at ~100 nm/s) corresponds to that being pulled back to the original position. This type of asymmetry was not observed in parallel microtubule pairs (blue columns). The pulled-back motion of the microtubule corresponds to rapid reduction of force observed in the force development recordings in (**A**), and is most likely due to dissociation of several crosslinking motor molecules from the microtubule lattice.

(**C**) The occurrence frequency of the rapid force reduction versus the length of microtubule overlap. Data indicates that such events tend to occur more frequently at shorter antiparallel microtubule overlap length. Plots are data from different microtubule pairs.

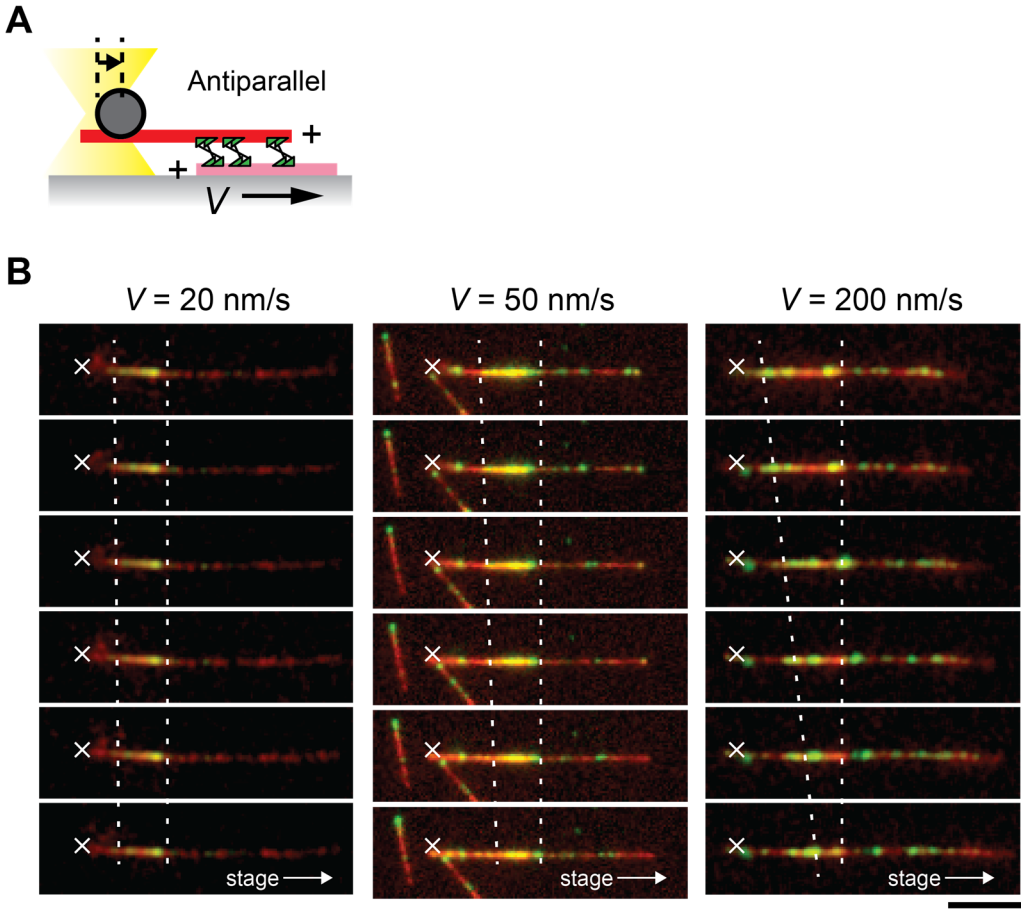

Figure S3 Additional analyses of force development within antiparallel microtubule pairs that are slid apart at constant velocity, Related to Figure 4

(**A**) Schematic showing the experimental set-up to measure force developed within sliding antiparallel microtubule pairs crosslinked by kinesin-5. The stage was moved at constant velocity (*V*). Microtubule polarity is marked (+).

(**B**) Representative time-lapse images showing motion of antiparallel microtubules (red) and localization of kinesin-5 (green). The stage was moved at the indicated velocity and in the direction indicated by white arrow. Trap position is marked (white 'x'). The region of filament overlap (between two dotted lines) decreased as the stage was moved further. Scale bar, 5 μm.

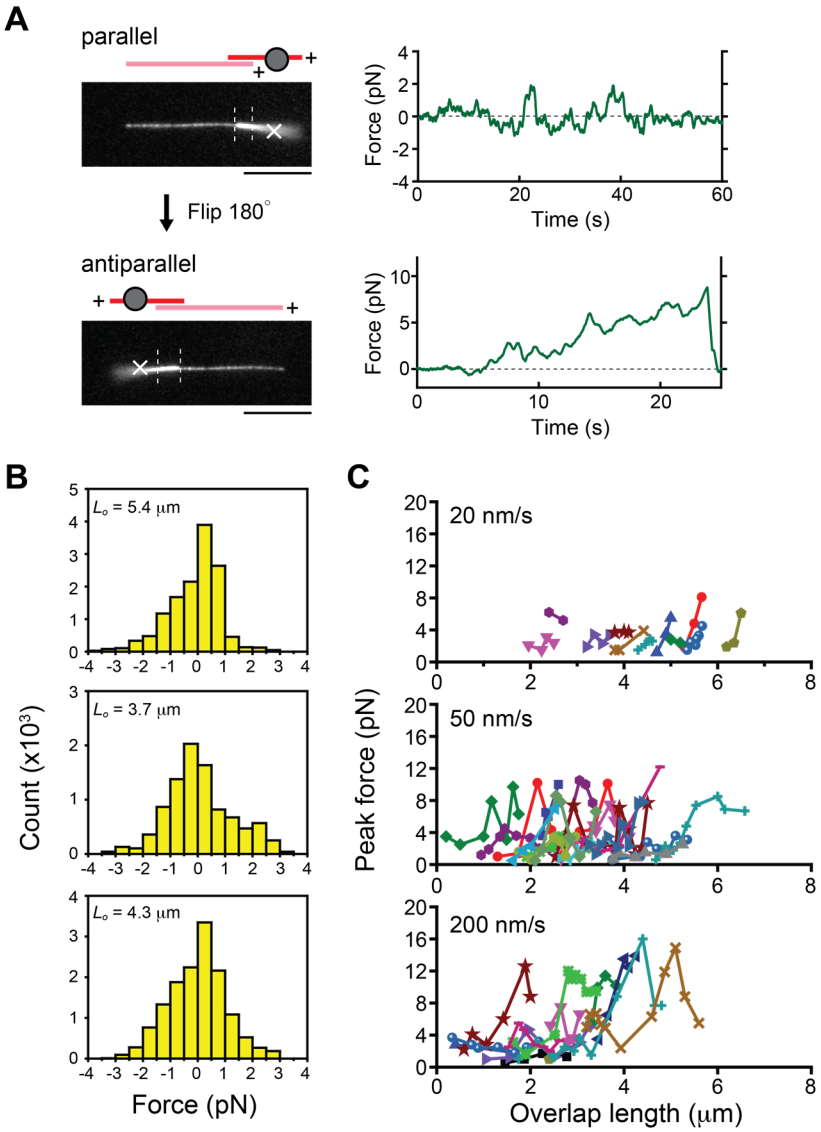

Figure S4 Additional analyses of parallel microtubule pairs crosslinked by kinesin-5, Related to Figure 5

(**A**) Microtubule 'flipping' assay. Fluorescence images show a parallel microtubule pair (upper image) to which a bead was attached and the force was measured (upper trace). The microtubule was then rotated by 180° and re-attached to the same surface microtubule (lower image). The force record obtained from the 'flipped' filament pair is shown (lower trace). Trap center is marked (white 'X'). Dashed lines indicate the region of filament overlap. Scale bars, 5 μm.

(**B**) Force distribution histograms of parallel microtubule pairs. Each histogram corresponds to the force recording data in Fig. 5B. The two end points in each histogram were used to estimate the maximum developed force.

(**C**) Peak force, measured for parallel microtubule pairs that were slid apart at indicated velocity, was plotted against the length of filament overlap. Colors indicate data from different microtubule pairs.

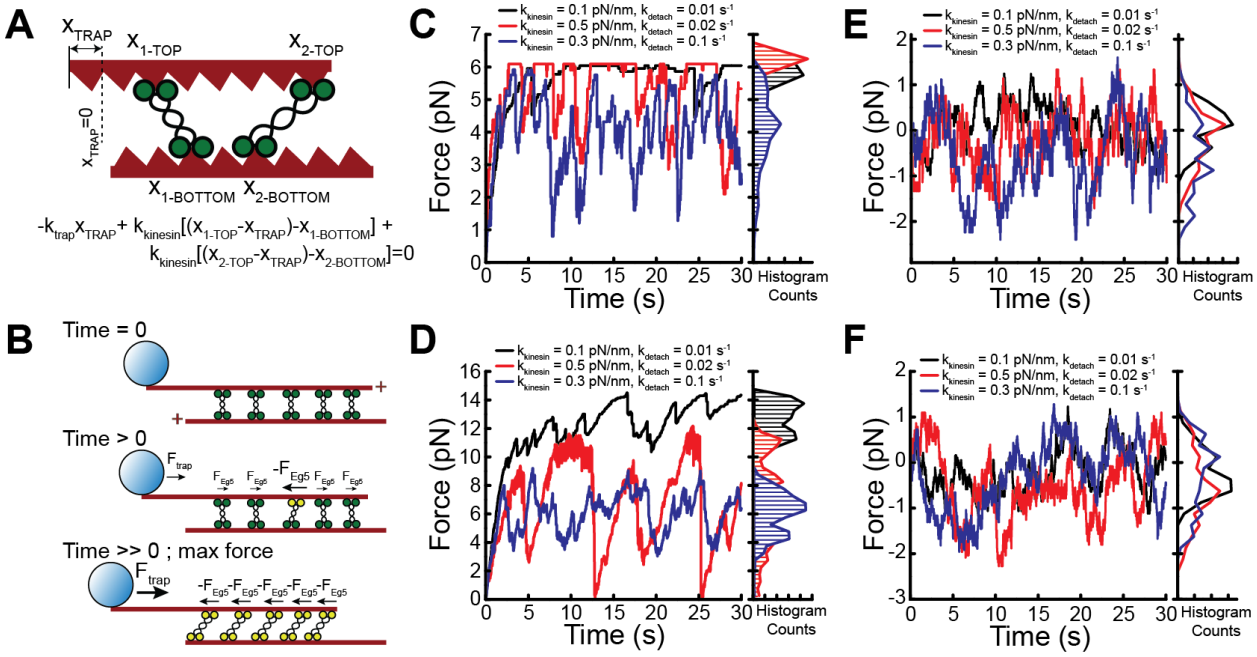

Figure S5. Model simulation results, Related to Figure 6

(**A**) Schematics detailing the force-balance formulation; the positions of each dimeric motor head on its microtubule substrate are given as $x_{i\text{-TOP}}$ and $x_{i\text{-BOTTOM}}$, respectively. Only two motors are presented for clarity. Note that while x_{TOP} and x_{BOTTOM} are discrete interger values (multiples of 8 nm, the periodicity of available kinesin binding sites on the microtubule), x_{TRAP} is a continuous variable. (**B**) Schematic illustrating various time points during the simulation. (**C-D**) Antiparallel sliding simulation sample results. (**C**) Time courses and force histograms for three individual anti-parallel sliding simulation trials at various values of $k_{kinesin}$ and k_{detach} for 4 motors. (**D**) Time courses and force histograms for three individual simulation trials at various values of $k_{kinesin}$ and k_{detach} for 10 motors. (**E-F**) Parallel sliding simulation sample results. (**E**) Time courses and force histograms for three individual parallel sliding simulation trials at various values of $k_{kinesin}$ and k_{detach} for 4 motors. (**F**) Time courses and force histograms for three individual simulation trials at various values of $k_{kinesin}$ and k_{detach} for 10 motors.

Supplementary Experimental Procedures

Reagents

Recombinant full-length *Xenopus laevis* kinesin-5-GFP was expressed and purified as described previously (Kwok et al., 2006). Tubulin was purified from bovine brain (Williams and Lee, 1982) and labeled either with biotin or X-rhodamine dye, using established methods (Hyman et al., 1991). These tubulins were co-polymerized with unmodified tubulin in a buffer comprised of 1 mM GMPCPP, 1 mM DTT and BRB80 (1 mM $MgCl_2$ 1 mM EGTA, 80 mM PIPES, pH 6.8). For biotinylated microtubules, biotin-tubulin, X-rhodamine tubulin and unmodified tubulin were mixed at the molar ratio of 1:1:20 (at ~3.9 μM final concentration); for non-biotinylated microtubules, these tubulins were mixed at the molar ratio of 0:1:10 (at ~3.6 μM final concentration). Following 2 h incubation at 37 °C, the polymerized microtubules were each stabilized by 20 μM Taxol and clarified by a centrifuge spin in TLA120.1. Rigor kinesin (G234A mutant, gift from Dr. Sarah Rice), used to establish a stable bead-microtubule attachment, was expressed and purified essentially as previously described (Rice et al., 1999). Prior to each force measurement assay, the purified rigor kinesin was mixed with carboxylated polystyrene microbeads (1 μm dia., cat. no. 08226, Polysciences Inc.) at the molar ratio of ~10^6:1 in 0.1 M Hepes buffer (pH 8.0). The mixture was then incubated for 20 min on ice and clarified by two cycles of centrifuge spins (9,000 ×g, 2 min each).

Microscope

Experiments were performed in an inverted microscope (Ti-U, Nikon), equipped with an EM-CCD camera (iXon DU-897, Andor), a closed-loop three-axis piezo stage (Nano LP-200, Mad City Labs), a force-calibrated optical tweezers, and a dual-mode TIRF and Epi-illumination optics. A high NA 100× objective (1.49 NA; CFI Plan Apo TIRF) was used for establishing both stable optical trapping and high-resolution fluorescence imaging.

Optical tweezers system was constructed based on a fiber-coupled infrared laser (1064 nm, CL1064, Crystalaser) and a position-sensitive detector (QP50-6SD2, Pacific Silicon Sensor). The laser beam was first collimated by a collimation optic (F260FC-C, Thorlabs) and expanded by ~2-fold using a pair of convex lenses. The beam was then passed through a 1:1 telescope, attenuated using neutral density filters, and merged into the microscope's light path using a dichroic IR flip mirror (z900dscp, Chroma) placed between the microscope's nose piece and the

fluorescence turret. Finally, the beam was introduced into the back aperture of the objective and focused to a diffraction-limited spot such that a micron-sized bead can be trapped near the sample plane. To monitor the displacement of the bead held in the optical tweezers, the laser beam passing through the sample plane was collected using an oil-immersion condenser (MEL41410, Nikon) and reflected out from the microscope's imaging path by a dichroic IR flip mirror (DMSP805L, Thorlabs). After passing through a long-pass optical filter (FEL0900), the beam was projected onto the quadrant photodiode detector placed at the back-focal plane of the objective (Allersma et al., 1998). The signals from each photodiode quadrant was amplified in a home-built signal amplifier and recorded using an in-house developed LabVIEW program via an AD converter (PCI-6251, National Instruments). The displacement signal along each coordinate was obtained by calculating the difference of the normalized signals between the adjacent quadrant pairs.

Fluorescence imaging system was built such that it allowed for two-color, near-simultaneous imaging of kinesin-5-GFP and X-rhodamine microtubules (<1 s time difference). Kinesin-5-GFP was imaged by TIRF using a 488 nm laser (Cyan, Spectra-physics) while X-rhodamine microtubules was imaged by epifluorescence using a mercury-arc light source (Intensilight, Nikon). These two excitation lights were, respectively, passed through a clean-up filter (FF01-482/563, Semrock) and an excitation filter (ET572/35x, Chroma), and then introduced into a combined TIRF/epifluorescence illuminator unit (Nikon) attached to the rear-port of the microscope. A dual-band dichroic filter (Di01-R488/561, Semrock) and a dual-band emission filter (59022m, Chroma) were placed in a fixed position of the microscope's fluorescence turret. Additionally, an IR-cut filter (KG3, Newport) was placed in front of the camera to reduce background light from the trapping laser. The emission of the imaging light source was controlled by mechanical shutters (MAC6000, Ludl), of which vibration noise associated with the shutter motion was eliminated by physically isolating them from the microscope. The images were acquired using NIS-Elements software (Nikon).

Assays

A) Measurement of kinesin-5 force within overlapping microtubules

Measurements of force generated by kinesin-5 crosslinking two microtubules were performed in a flow chamber (~10 µl, = 1 volume) assembled by adhering two strips of double-sided tape onto

a clean glass slide onto which a coverslip coated with PEG and biotin-PEG was layered (Subramanian et al., 2013). The chamber was first incubated with 0.5 mg/ml α-casein for 3 min to block uncoated surface, followed by 0.2 mg/ml neutravidin for 5 min to provide linkages on biotin-PEG. Subsequently, biotinylated microtubules were infused and incubated for 10 min. After each step the chamber was flushed with >3 volumes of wash buffer (BRB80, 1 mM DTT and 20 μM Taxol). Finally, the chamber was filled with motility sample (non-biotinylated microtubules, 1 nM kinesin-5-GFP, 2 mM ATP, 3 mM $MgCl_2$, 1 mM EGTA, 60 mM PIPES (pH 6.8), 4.5 mg/ml glucose, 350U/ml glucose oxidase, 34U/ml catalase, 0.5 mg/ml α-casein, 1 mM DTT, 20 μM Taxol and ~0.1 pM beads) and sealed with VaLaP.

To measure force, an optically-trapped bead was attached to near the free-end of a non-biotinylated microtubule in a microtubule 'sandwich' assembled on coverslip surface. The bead was attached close (2-5 μm) to the region of two microtubule overlap such that the bead-attached microtubule was prevented from buckling due to pushing force generated by kinesin-5. The contact between the bead and the surface microtubule was also avoided. The bead position was recorded using the position-sensitive detector at the sampling rate of 0.1-0.5 kHz. Microtubules and kinesin-5-GFP were time-lapse imaged (interval: 1-5 s; exposure time: 200-300 ms), in parallel with the force measurement. For microtubule pulling experiments (Figure 4 and 5H-L), the piezo stage was moved at constant velocity soon after the kinesin-5 dependent force reached a steady state. Measurements were performed at room temperature (20-23 °C) and completed within 15 min, a time interval over which no significant change in kinesin-5-GFP motility was observed (data not shown). Throughout the measurement, the trapped bead was kept at ~1 μm above coverslip surface, at which the trap stiffness, calibrated using a viscous drag method (Svoboda and Block, 1994), was 0.065 pN/nm. The stiffness was approximately linear over ±250 nm from the trap center in x-y plane (n = 5 beads) and kept <8% variability in the range 0.5-2.0 μm above coverslip surface (n = 4 beads).

Polarity of microtubules was determined based on the relative sliding velocity measured prior to the bead attachment, as antiparallel microtubules slid apart at >40 nm/s velocity and parallel microtubules remained relatively static (<10 nm/s). These two populations were found with roughly equal probability as reported previously (Hentrich and Surrey, 2010; Kapitein et al., 2005).

B) Rupture-based counting

To estimate how many kinesin-5 molecules are involved in crosslinking two microtubules, we used the optical trap to rapidly disrupt motor-filament interactions and count the number of 'rupture' events associated with the filament separation (Nishizaka et al., 1995) (Figure 1F-H). To achieve this, the piezo stage was moved at constant velocity while the trap position was held at a fixed position such that one end of the filament was pulled orthogonal to the other. The stage was moved at a fast velocity (0.3 μm/s) such that the two microtubules were fully separated while the relative filament sliding was kept at minimum. The motion of the trapped bead was recorded at 0.5 kHz and analyzed to determine the number of rupture events (see below). In the absence of kinesin-5, no prominent rupture signals were observed while pulling one filament over the coverslip surface prepared in a similar way; therefore, non-specific interactions such as those arising between microtubules and with coverslip surface should be negligibly small.

C) Microtubule flipping assay

The microtubule flipping experiments, shown in Figure 5C and Figure S4, was performed as follows. First, the force developed within a microtubule pair crosslinked by kinesin-5 was measured as described above. The microscope stage was then moved in a way similar to what we have done for the rupture-based counting, such that the surface microtubule was detached from the bead-held microtubule. Following the full separation of the filaments, the orientation of the bead-held microtubule was flipped 180° by applying fluid flow to the filament, using a relatively fast and transient motion of the piezo stage. The contact of the optically-trapped bead with any microtubules in solution and on coverslip surface was avoided. The surface microtubule was then brought into contact with the bead-held microtubule, and the force developed within the newly assembled filament pair was measured.

C) Measurement of single kinesin-5 force

To examine how much force the single kinesin-5 molecule can generate, we performed a 'conventional' force assay by attaching our kinesin-5 construct to a microbead and measured force as it moves along single microtubules (Figure 3D-F). To this end, carboxylated microbeads were first coated with anti-GFP antibody according to a manufacturer's protocol (#644, Polysciences, Inc.). Following two cycles of clarifying centrifuge spins, the pre-coated beads (~4

pM) were mixed with the full-length kinesin-5-GFP at a range of motor protein concentrations (0.25 nM to 25 nM). After 5-min incubation of each reaction on ice, the bead-motor conjugate was captured using optical tweezers, brought into contact with surface-immobilized microtubules such that the developed force was measured by monitoring the displacement of the bead from trap center. The assay was performed in the buffer of which composition was essentially the same as in the measurement of kinesin-5 force within overlapping microtubules.

Data Analysis

A) Developed force

To determine the extent of the maximum force developed in each microtubule pair, the individual force development record, acquired at 0.1 kHz sampling rate, was first smoothened by a 200-ms moving average filter. For antiparallel microtubule pairs, the smoothened trace was processed to determine the force plateau, which was defined as the region where the force signal was maintained at a steady level for >1 s without significant fluctuation (<10% change in average force). In case of multiple force plateaus, these force values were averaged. For parallel microtubule pairs that typically exhibited bidirectional force fluctuation, the smoothened trace was processed to generate a histogram with 0.25 pN bin width, and then the maximum developed force was determined by averaging the values of the two end columns of the histogram. For microtubule pulling experiments in Figure 4 and 5H-L, the extent of resisting force developed in each filament pair was estimated by calculating the average force developed at each 0.5 μm bin of the microtubule overlap length determined as below. Data were analyzed in Microsoft Excel and OriginPro.

B) Microtubule overlap length

The amount of overlap between two microtubules was estimated by performing a linescan analysis along the long axis of the microtubules. The line width of 3 pixels (= 0.45 μm) was used to generate an intensity profile, in which the overlap length was determined by measuring the end-to-end distance of a region where the X-rhodamine signal intensity was double the average intensity of microtubules measured in the non-overlapping region. For microtubule pulling experiments in Figure 4 and 5H-L, the length of microtubule overlap (L) at each time point t was estimated according to $L = L_0 - V \cdot t + \Delta x$, where L_0, V, Δx are the initial overlap length, the stage

velocity and the displacement of the trapped bead from trap center, respectively. The image analyses were performed in Image J.

C) Motor number

The number of kinesin-5 molecules within a microtubule overlap was estimated based on the total fluorescence intensity of kinesin-5-GFP localized within the overlap region divided by the average GFP signal of single kinesin-5-GFP. The total GFP intensity was estimated using a rectangular ROI drawn to cover the entire microtubule overlap followed by background subtraction. The bleed-through of the X-rhodamine to GFP channel was corrected based on the pre-determined bleed-through efficiency per micron microtubule and the length of the microtubule overlap analyzed (typically <10%). On the other hand, to determine the average fluorescence intensity of single kinesin-5-GFP (Figure S1A), our kinesin-5 construct was passively adsorbed onto a coverslip surface at a low density (10-20 molecules per field). The individual GFP spots were detected using Image J Mosaic Plugins, and then the fluorescence intensity of each detected spot was measured and background subtracted. Finally, the data from several different fields and from several chambers were pooled and averaged.

To estimate the number of crosslinking motor protein molecules, the bead displacement record obtained from the rupture-based analysis was first processed by 100-ms moving average filter. A pairwise distance was then calculated at two endpoints of a window moving along the averaged bead displacement record (window size: 200 ms). A threshold level was set at three-fold of the standard deviation of the reference pairwise distance signal, which was calculated from the data acquired before moving the stage, and the pairwise distance signal that exceeded the threshold was defined as a 'rupture". The detection threshold was well above the resolution that should distinguish single-head and double-head binding modes of kinesins (Uemura et al., 2002); therefore, each rupture event most likely corresponds to the full detachment of the tetrameric molecule and not due to the unbinding of one motor head within the dimeric motor pair.

Detailed Description of Simulations

(1.) (a) Stepping behavior of a single dimeric kinesin-5 motor protein

It has been shown that the velocity of a dimeric kinesin motor protein stepping along its

microtubule track can be well described by a Michaelis-Menten kinetic scheme (Visscher et al., 1999):

$$\text{Kinesin5} + \text{ATP} \underset{k_{off}}{\overset{k_{on}}{\rightleftharpoons}} \text{Kinesin5} \cdot \text{ATP} \overset{k_{cat}}{\rightharpoonup} \text{Kinesin5} + \text{ADP} + \text{P}_\text{i}$$

where k_{on} is the rate of ATP binding to the kinesin-5 motor, k_{off} is the rate of ATP unbinding, and k_{cat} is the rate of ATP hydrolysis; this model assumes that the hydrolysis step is irreversible. The velocity is thus related to these rates and the ATP concentration by:

$$V = \frac{V_{max}[ATP]}{[ATP] + K_m}$$

where $K_m = \frac{k_{cat}+k_{off}}{k_{on}}$. The maximum velocity V_{max} at saturating ATP concentrations and under zero applied load can be then given by $V_{max} = k_{cat} * x$, where x = 8 nm, the kinesin step size.

When a resisting force is applied to the motor protein, this velocity is modulated until it reaches zero at the stall force. This can be represented by adding a force dependence term as $V_{max} = k_{cat} * x * \varepsilon(F)$, where ε($F$) can be either linear (which we assume here) or a more complex formulation, depending on the motor's force-velocity relationship, with the requirement that ε(0) = 1 and ε(F_0) = 0. For many kinesins, K_m depends on the applied force as well. We therefore allow k_{off} to vary with force via an Arrhenius-like term. Finally, the rate of detachment of the motor protein, k_{detach}, from the microtubule surface can depend on applied force, and we can define a force-independent parameter k_{attach} which is the rate at which an unbound motor domain can reattach to the microtubule surface.

(b) Diffusive mode of tetrameric kinesin-5

The full-length tetrameric kinesin-5 protein has been shown to contain both motor and non-motor microtubule binding domains, with two pairs of each at opposite ends of the molecule. It is possible for kinesin-5 to bind to the microtubule surface via the non-motor domain alone, during which time the molecule can undergo quasi-1D diffusion along the surface (Weinger et al., 2010). We therefore consider a scenario wherein the motor domains, but not the

non-motor domain, can disengage from the surface at a rate $k_{switch\text{-}diffuse}$ and the molecule is free to diffuse with a rate $k_{diffuse}$. Reported values for the diffusion constant ($D \sim 2 * 10^3$ nm^2/s) measured under similar buffer conditions for the construct employed in this study were used to derive $k_{diffuse}$. $K_{diffuse}$ is additionally modulated by the application of force using an Arrhenius-like term. From this diffusive state, the protein can either fully detach (with rate k_{detach}) from the microtubule surface, or the motor domains can reengage with a rate $k_{reengage}$.

Given these collective assumptions, we can simulate the force and ATP dependent stepping behavior of a single processive kinesin motor using the following values:

$$\mathrm{kon} = 8.9 * 10^5\ \mathrm{M^{-1}s^{-1}}$$

$$[\mathrm{ATP}] = 2\mathrm{mM}$$

$$\mathrm{k_{off}}(0) = 8\ \mathrm{s^{-1}}$$

$$\mathrm{k_{cat}} = 3\ \mathrm{s^{-1}}$$

$$\mathrm{k_{off}}(\mathrm{F}) = \mathrm{k_{off}}(0) * \mathrm{e}^{\frac{\mathrm{F}*2\mathrm{nm}}{\mathrm{kT}}}$$

$$k_{detach}(F) = k_{detach}(0) * \mathrm{e}^{\frac{\mathrm{F}*1\mathrm{nm}}{\mathrm{kT}}}$$

$$k_{attach} = 10\ s^{-1}$$

$$k_{switch-diffuse} = 0.1\ s^{-1}$$

$$k_{reengage} = 10\ s^{-1}$$

$$k_{diffuse} = 30\ s^{-1}$$

$$stall\ force\colon \mathrm{F_0} = 1.5\mathrm{pN}$$

$$\epsilon(\mathrm{F}) = 1 - \frac{\mathrm{F}}{\mathrm{F_0}}$$

(2.) Tetrameric kinesin-5 crosslinking two microtubules

To describe the behavior of a tetrameric kinesin-5 motor protein which is crosslinking two microtubules, we consider two independent dimeric motor domains (possessing stepping and diffusive properties as described above) connected by a spring-like linker region which stretches as the two heads become spatially separated as they move along the microtubule. This parameter $k_{kinesin}$ is varied such that each head can take from one to many steps towards its respective microtubule plus-end before a force large enough to stall the motor protein is generated across the tetramer. We use a simple linear spring constant term, which does not take directly into

account the elastic modulus of the coiled-coil linker domain or rotational torque applied to the motor heads, but instead coarsely defines an energy penalty for the spatial separation of the pairs of motor domains.

(3.) Distribution of forces across motors with optically trapped microtubule end

The central feature of our simulation is the balance of forces across the motors with the optically trapped microtubule end serving as a linear spring providing resistance to the microtubule motion (Supplementary Fig. 5A, B). For a given number of motors, we require that the forces must balance according to:

$$F_{trap} = \sum F_{kinesin}$$

By appropriately defining the coordinates of discrete (i.e., 8 nm spacing) motor positions along the free ('top') microtubule and the discrete positions along the immobilized 'bottom' microtubule, as well as considering the position of the moving free microtubule end (which is equivalent to the optical trap position, x_{trap}), we can rewrite this relationship as:

$$-k_{trap}x_{trap} + \sum_{i}^{N}\left(k_{kinesin} * \left[\left(x_{i\,TOP} - x_{trap}\right) - x_{i\,BOTTOM}\right]\right) = 0$$

Solving for x_{trap} yields:

$$-\frac{k_{trap}}{k_{kinesin}}x_{trap} - Nx_{trap} + \sum_{i}^{N} x_{i\,TOP} - \sum_{i}^{N} x_{i\,BOTTOM} = 0$$

$$\left(N + \frac{k_{trap}}{k_{kinesin}}\right)x_{trap} = \sum_{i}^{N} x_{i\,TOP} - \sum_{i}^{N} x_{i\,BOTTOM}$$

$$x_{trap} = \frac{\sum_{i}^{N} x_{i\,TOP} - \sum_{i}^{N} x_{i\,BOTTOM}}{\left(N + \frac{k_{trap}}{k_{kinesin}}\right)}$$

Thus, the position of the microtubule end (trap position, x_{trap}) will depend on the relative positions along the microtubules of each motor head, the total number of motors engaged in

force generation, and both the trap and kinesin stiffness.

Monte Carlo Simulations

(A) Anti-parallel sliding

Start at Time = 0 s with all kinesin-5 molecules in a fully relaxed state, (i.e., with all $Force_{kinesin\text{-}5}$ = 0 pN) as well as $Force_{trap}$ = 0 pN.

At each subsequent time step, perform the following:

1.) For each motor, check the attachment state of both the top and bottom heads.
    a. If the head is fully detached, reattach if rand() < k_{attach}*Δt, setting the position on the microtubule such that the Force calculated across the motor is as close to zero as possible (i.e., achieves the condition $k_{kinesin}$ * [(x_{top}-x_{trap})-x_{bottom}] = 0).
    b. If the head is attached, detach if rand() < $k_{detach}(F)$*Δt. If head detaches, set ATP state to 0, and set the force across the tetramer = 0 pN, until reattachment.
    c. If the head is attached but did not detach after step (b), allow the molecule to enter a diffusive state if rand() < $k_{switch\text{-}diffuse}(F)$*$\Delta t$. If the molecule is in a diffusive state, allow it to switch back to a motor-engaged state if rand() < $k_{reengage}$*Δt.
    d. In all instances, if rand() > Probability, do nothing and move to the next head.
2.) For each engaged (e.g. non-diffusive, attached) motor, check the ATP binding state of both the top and bottom heads:
    a. If the ATP binding state is empty, let an ATP bind if rand()<k_{on}*[ATP]* Δt.
    b. If the ATP binding state is occupied, let the ATP unbind if rand()<$k_{off}(F)$* Δt.
    c. In both instances, if rand() > Probability, do nothing and move to the next head.
3.) For each head in a diffusive state:
    a. Allow the head to 'hop' in the direction of force application if rand()<$k_{diffuse}$*exp(F*(4 nm)/kT) or in the direction opposite force application if rand()>1-($k_{diffuse}$*exp(-F*(4 nm)/kT)).
    b. If neither condition is met, allow the head's position to remain unchanged.
4.) For each engaged motor, if the ATP binding site is occupied:
    a. If the Force across the motor < Stall Force:

i. If rand()<k_{cat}* Δt, the ATP hydrolyzes and the motor steps 8nm along the microtubule towards its plus-end if rand()<ε(F); the ATP binding state is set to 0 (empty)
ii. If rand()>Probability, do nothing and move to the next head

b. If the Force across the motor > Stall Force:
i. If rand()<k_{cat}* Δt, the ATP hydrolyzes and the motor steps 8nm backwards along the microtubule towards its minus-end if rand()<(F/F_0)-1; the ATP binding state is set to 0 (empty)
ii. If rand()>Probability, do nothing and move to the next head

5.) Determine the number of motors that have both heads attached, $N_{engaged}$.

6.) Calculate the new position of the trap according to:

$$x_{trap} = \frac{\sum_1^N (x_{i\ TOP\ attach} * x_{i\ TOP}) - \sum_1^N (x_{i\ BOTTOM\ attach} * x_{i\ BOTTOM})}{N_{engaged} + \frac{k_{trap}}{k_{kinesin}}}$$

7.) Calculate the Force across each attached motor according to:

$$\text{Force}_i = k_{kinesin} * x_{attach_i} * \left(x_{pos_{TOPi}} - x_{trap} + x_{pos_{BOTTOM\_i}}\right)$$

Repeat steps 1-6 with updated values for Force per motor for desired length of time (typically 30-90 seconds).

(B) Parallel Sliding

In the case of parallel sliding, we allow both dimeric motor head units to actively walk along their respective microtubule tracks towards plus-ends. Therefore, this mode is identical in practice to the anti-parallel situation detailed above, except for the fact that the directionality of 'bottom' head stepping is reversed. That is, rather than a step occurring after ATP hydrolysis moving the motor by -8nm (to the left on the bottom microtubule in Supplementary Fig. 5A), the motor steps +8 nm (to the right). All other model parameters remain the same. Importantly, we do not include a torsional energy penalty, which could account for the 180° rotation the tetramer must undergo, relative to the antiparallel case, in order to bind both of the parallel microtubules.

(C) Moving microtubules

The steps of the simulation remain identical in the case of actively moving microtubules (both parallel and antiparallel), except that (1) the positions of the bottom 'fixed' microtubule are incremented linearly at the indicated rate (e.g. 25, 50, 100, or 200 nm/s) and (2) the density of available motor proteins per unit length is held fixed (e.g. 2 proteins per micron). Therefore, as the region of overlap decreases with time, so too does the number of maximum possible motor proteins. We begin the simulations with a maximum overlap length of 6 microns, consistent with the maximum overlap length compatible with the experimental assays. The overlap length is reduced in a nearly linear manner until it reaches zero, at which point no motors are available to crosslink the microtubule pair and the force on the free microtubule as measured by the bead falls to zero.

Supplementary References

Allersma, M.W., Gittes, F., deCastro, M.J., Stewart, R.J., and Schmidt, C.F. (1998). Two-dimensional tracking of ncd motility by back focal plane interferometry. Biophysical journal *74*, 1074-1085.

Hentrich, C., and Surrey, T. (2010). Microtubule organization by the antagonistic mitotic motors kinesin-5 and kinesin-14. The Journal of cell biology *189*, 465-480.

Hyman, A., Drechsel, D., Kellogg, D., Salser, S., Sawin, K., Steffen, P., Wordeman, L., and Mitchison, T. (1991). Preparation of modified tubulins. Methods in enzymology *196*, 478-485.

Kapitein, L.C., Peterman, E.J., Kwok, B.H., Kim, J.H., Kapoor, T.M., and Schmidt, C.F. (2005). The bipolar mitotic kinesin Eg5 moves on both microtubules that it crosslinks. Nature *435*, 114-118.

Kwok, B.H., Kapitein, L.C., Kim, J.H., Peterman, E.J., Schmidt, C.F., and Kapoor, T.M. (2006). Allosteric inhibition of kinesin-5 modulates its processive directional motility. Nature chemical biology *2*, 480-485.

Nishizaka, T., Miyata, H., Yoshikawa, H., Ishiwata, S., and Kinosita, K., Jr. (1995). Unbinding force of a single motor molecule of muscle measured using optical tweezers. Nature *377*, 251-254.

Rice, S., Lin, A.W., Safer, D., Hart, C.L., Naber, N., Carragher, B.O., Cain, S.M., Pechatnikova, E., Wilson-Kubalek, E.M., Whittaker, M.*, et al.* (1999). A structural change in the kinesin motor protein that drives motility. Nature *402*, 778-784.

Subramanian, R., Ti, S.C., Tan, L., Darst, S.A., and Kapoor, T.M. (2013). Marking and measuring single microtubules by PRC1 and kinesin-4. Cell *154*, 377-390.

Svoboda, K., and Block, S.M. (1994). Force and velocity measured for single kinesin molecules. Cell *77*, 773-784.

Uemura, S., Kawaguchi, K., Yajima, J., Edamatsu, M., Toyoshima, Y.Y., and Ishiwata, S. (2002). Kinesin-microtubule binding depends on both nucleotide state and loading direction. Proceedings of the National Academy of Sciences of the United States of America *99*, 5977-5981.

Visscher, K., Schnitzer, M.J., and Block, S.M. (1999). Single kinesin molecules studied with a molecular force clamp. Nature *400*, 184-189.

Williams, R.C., Jr., and Lee, J.C. (1982). Preparation of tubulin from brain. Methods in enzymology *85 Pt B*, 376-385.